Intranasal SARS-CoV-2 RBD decorated nanoparticle vaccine enhances viral clearance in the Syrian hamster model

Patel DR[1,4], Minns AM[2,4,6], Sim DG[3,4], Field CJ[1,2], Kerr AE[1,4], Heinly T[1,4], Luley EH[1,5], Rossi, R.M. [4], Bator, C.[4], Moustafa, I.M.[2], Hafenstein SL[2,4,7], Lindner SE[2,4,6*], Sutton TC[1,4*]

[1] Department of Veterinary and Biomedical Sciences, Pennsylvania State University

[2] Department of Biochemistry and Molecular Biology, Pennsylvania State University

[3] Department of Biology, Pennsylvania State University

[4] The Huck Institutes of Life Sciences, Pennsylvania State University

[5] Animal Diagnostic Laboratory, Pennsylvania State University

[6] The Huck Center for Malaria Research

[7] Department of Medicine, Pennsylvania State University

* Co-corresponding Authors:

Corresponding Authors:

Scott E. Lindner, Ph.D.

W230B Millennium Science Complex

University Park, PA 16802

P: +1.814.867.4062

E: Scott.Lindner@psu.edu

ORCID: 0000-0003-1799-3726

Troy C Sutton, Ph.D.

W229A Millennium Science Complex

University Park, PA 16802

P: +1.814.863.0693

E: tcs38@psu.edu

ORCID: 0000-0002-7880-4784

ABSTRACT

Multiple vaccines have been developed and licensed for SARS-CoV-2. While these vaccines reduce disease severity, they do not prevent infection, and SARS-CoV-2 continues to spread and evolve. To prevent infection and limit transmission, vaccines must be developed that induce immunity in the respiratory tract. Therefore, we performed proof-of-principle vaccination studies with an intranasal nanoparticle vaccine against SARS-CoV-2. The vaccine candidate consisted of the self-assembling 60-subunit I3-01 protein scaffold covalently decorated with the SARS-CoV-2 receptor binding domain (RBD) using the SpyCatcher-SpyTag system. We verified the intended antigen display features by reconstructing the I3-01 scaffold to 3.4A using cryo-EM, and then demonstrated that the scaffold was highly saturated when grafted with RBD. Using this RBD-grafted SpyCage scaffold (RBD+SpyCage), we performed two unadjuvanted intranasal vaccination studies in the “gold-standard” preclinical Syrian hamster model. Hamsters received two vaccinations 28 days apart, and were then challenged 28 days post-boost with SARS-CoV-2. The initial study focused on assessing the immunogenicity of RBD+SpyCage, which indicated that vaccination of hamsters induced a non-neutralizing antibody response that enhanced viral clearance but did not prevent infection. In an expanded study, we demonstrated that covalent bonding of RBD to the scaffold was required to induce an antibody response. Consistent with the initial study, animals vaccinated with RBD+SpyCage more rapidly cleared SARS-CoV-2 from both the upper and lower respiratory tract. These findings demonstrate the intranasal SpyCage vaccine platform can induce protection against SARS-CoV-2 and, with additional modifications to improve immunogenicity, is a versatile platform for the development of intranasal vaccines targeting respiratory pathogens.

53 **IMPORTANCE**

54 Despite the availability of efficacious COVID vaccines that reduce disease severity, SARS-CoV-
55 2 continues to spread. To limit SARS-CoV-2 transmission, the next generation of vaccines must
56 induce immunity in the mucosa of the upper respiratory tract. Therefore, we performed proof-of-
57 principle, unadjuvanted intranasal vaccination studies with a recombinant protein nanoparticle
58 scaffold, SpyCage, decorated with the receptor-binding domain (RBD) of the S protein
59 (SpyCage+RBD). We show that SpyCage+RBD was immunogenic and enhanced SARS-CoV-2
60 clearance from the nose and lungs of Syrian hamsters. Moreover, covalent grafting of the RBD
61 to the scaffold was required to induce an immune response when given via the intranasal route.
62 These proof-of-concept findings indicate that with further enhancements to immunogenicity
63 (e.g., adjuvant incorporation, antigen optimization), the SpyCage scaffold has potential as a
64 versatile, intranasal vaccine platform for respiratory pathogens.

65

66 **INTRODUCTION**

67 Severe acute respiratory syndrome coronavirus- 2 (SARS-CoV-2) is the etiological agent of the
68 coronavirus disease 2019 (COVID-19)[1] pandemic. SARS-CoV-2 is an enveloped
69 betacoronavirus with a non-segmented positive-sense single-stranded RNA genome. The
70 genome encodes 4 structural proteins: spike (S), membrane (M), envelope (E), and
71 nucleocapsid (N), as well as multiple non-structural proteins[2]. The S protein is the major surface
72 protein and mediates viral entry and fusion. The receptor-binding domain (RBD) of the S
73 protein binds the host receptor angiotensin-converting enzyme 2 (ACE2), leading to endocytosis
74 of the virion and infection of the host[2,3]. Importantly, antibody responses against SARS-CoV-2 in
75 humans and experimentally infected animals are predominantly directed toward the S protein.
76 Moreover, titers of RBD-binding antibodies correlate with neutralizing activity, and RBD is
77 considered the immunodominant region of the S protein [4,5]. Therefore, RBD represents a

78 suitable immunogen for vaccine development, and blocking this domain has the potential to
79 prevent infection.
80 Prior to the SARS-CoV-2 pandemic, vaccines targeting coronaviruses in humans had not been
81 advanced through late-stage clinical trials. Development of multiple SARS-CoV-2 vaccine
82 candidates was enabled by rapid sequencing of the viral genome as well as pre-existing
83 knowledge about vaccination against severe acute respiratory syndrome coronavirus (SARS-
84 CoV) and Middle Eastern respiratory syndrome coronavirus (MERS-CoV)[6]. Currently, there are
85 at least 12 vaccines approved for human use [7,8]. Licensed vaccines such as CoronaVac and
86 QazCovid-in contain inactivated virus [9-13], while vaccines developed by Pfizer/BioNTech and
87 Moderna consist of mRNA encoding the pre-fusion S protein enclosed in a lipid nanoparticle[14].
88 The Novavax vaccine contains recombinant S protein, and vaccines from Johnson & Johnson
89 and AstraZeneca use viral vectors to deliver DNA encoding the S protein[15]. Importantly, all of
90 these licensed vaccines are delivered by intramuscular (*i.m.*) injection, and these vaccines have
91 been shown to reduce the severity of SARS-CoV-2 infection[11,16,17]; however, these vaccines do
92 not prevent infection, and vaccinated individuals can develop symptomatic infections and
93 transmit the virus onwards.
94 Intramuscular vaccination induces a systemic immune response with high titers of IgG
95 antibodies that enter the lungs to reduce viral replication and disease severity[6,18]. However, the
96 delivery of vaccines via the *i.m.* route does not induce a strong mucosal immune response[6], and
97 a mucosal response is required to prevent infection of the upper respiratory tract and limit
98 transmission. In contrast to *i.m.* administered vaccines, an efficacious intranasal vaccine has
99 the potential to protect mucosal surfaces via the induction of secretory IgA antibodies and
100 mucosal T cells. Moreover, these vaccines can also induce a serum IgG response that can
101 impart similar disease reductions as observed for existing vaccines (reviewed in [19]). However,
102 on-going analyses of licensed SARS-CoV-2 vaccine efficacy has shown that vaccine-induced
103 immunity wanes over time, resulting in breakthrough infections [20-22]. In addition, intranasal

104 administration of mRNA vaccines to mice did not confer protection against SARS-CoV-2
105 challenge[23]. As a result, there is a growing need to develop a second generation of SARS-CoV-
106 2 vaccines that can be administered through intranasal routes to induce protective mucosal
107 immunity [24,25].
108 To date, a limited number of intranasal vaccine candidates have been developed against SARS-
109 CoV-2. Most of these candidates are viral vectors or live-attenuated vaccines; however, there
110 have been safety concerns with viral vectored SARS-CoV-2 vaccines, and their administration is
111 limited to individuals older than 18 years of age[26,27]. Moreover, the only licensed live-attenuated
112 intranasal vaccine is against influenza, and due to safety concerns and poor immunogenicity in
113 older individuals, its use is restricted to individuals 2-49 years of age[28]. Therefore, there is a
114 need to develop intranasal vaccines that would be suitable for individuals of all ages.
115 To address this gap, we adapted the I3-01 self-assembling protein into a nanoparticle bearing a
116 flexible SpyCatcher domain (SpyCage) to display SARS-CoV-2 RBD/SpyTag (RBD+SpyCage)
117 as an intranasal vaccine. The I3-01-based platform has been shown to be an excellent
118 immunization scaffold to present a variety of antigens from viral (SARS-CoV-2, influenza, EBV,
119 CSFV) and parasitic (*Plasmodium*) pathogens that reproducibly boosts immune responses as
120 compared to the unscaffolded antigen[29-36]. However, these trials have been restricted to *i.m.*
121 injections with immune responses as endpoint readouts, with a few notable studies proceeding
122 through challenges with live pathogens[35,37].
123 Here we performed proof-of-principle studies to evaluate RBD grafted to the SpyCage scaffold
124 (RBD+SpyCage) as an intranasal vaccine in the “gold-standard” Syrian hamster model. Syrian
125 hamsters are highly permissive to SARS-CoV-2 infection, and the virus efficiently transmits in
126 these animals by direct contact and respiratory droplets (*i.e.,* airborne transmission)[38-40]. We
127 performed two separate efficacy studies in which hamsters were given a prime and boost
128 intranasal vaccination and challenged with SARS-CoV-2. We demonstrated covalent grafting of
129 RBD to SpyCage was required to induce an IgG antibody response in vaccinated animals. Upon

130 SARS-CoV-2 challenge, regardless of vaccination status, all hamsters became infected and
131 exhibited weight loss; however, animals vaccinated with RBD+SpyCage more rapidly cleared
132 the virus from both the upper and lower respiratory tract with evidence of reduced lung
133 pathology. Collectively, these studies demonstrate the potential for SpyCage as the basis of an
134 intranasal vaccine platform for SARS-CoV-2 and possibly other respiratory pathogens.

135 **MATERIALS AND METHODS**

136 ***Production and Purification of Apo Cage and SpyCage***

137 The Apo Cage scaffold is based upon the 6xHis/I3-01 protein described previously by Hsia and
138 colleagues[41,42]. The SpyCage scaffold consists of a genetic fusion of a 6xHis tag, the
139 SpyCatcher domain, a flexible linker, and the I3-01 protein[41,43]. These proteins were expressed
140 in the *E. coli* BL21 (DE3) CodonPlus strain bearing either plasmid pSL1013 (Apo Cage) or
141 pSL1040 (SpyCage) using a modified pET28 vector. Cultures were grown in LB media at 37ºC
142 to an OD600 of ~0.5, at which point protein expression was induced by the addition of 0.5mM
143 IPTG (final concentration) for 2.5 hours. Cell pellets were suspended in 50mL of resuspension
144 buffer (50 mM Tris-Cl pH8.0 at room temperature(RT), 500 mM NaCl) per 1L of culture, and
145 cells were lysed by sonication using a disruptor horn attachment, using three pulses of 30
146 seconds each at 70% amplitude and 50% duty cycle (model 450 Branson Digital Sonifier). The
147 crude extract was spun at 15,500 *xg* for 20 minutes at 4C, and the soluble fraction was then
148 incubated in batch with 2 ml of equilibrated Ni-NTA resin for 1 hour at 4C. The resin was applied
149 to a gravity flow column and washed with 50 mL of resuspension buffer followed by 50 mL of
150 Mid-Imidazole buffer (25 mM Tris-Cl pH7.5@RT, 500 mM NaCl, 50 mM Imidazole, 250 mM
151 dextrose, 10% v/v glycerol). Apo cage and SpyCage protein were eluted using elution buffer (50
152 mM Tris-Cl pH8.0@RT, 500 mM NaCl, 300 mM imidazole), and then were exhaustively dialyzed
153 into 50 mM Tris-Cl pH8.0@RT, 500 mM NaCl, 1 mM DTT, 10% v/v glycerol. The dialyzed
154 material was then concentrated to ~2.0 mg/ml using Amicon Ultra Centrifugal Filters (Fisher
155 Scientific Cat#: UFC9-003-08) and snap-frozen in liquid nitrogen for long-term storage at -80C.
156 Complete plasmid sequences are provided in Supp File 1.

157

158 ***Production and Purification of SARS-CoV-2 Spike RBD***

159 The Receptor-Binding Domain (RBD) of SARS-CoV2-2 Spike protein was produced with and
160 without a C-terminal SpyTag for covalent attachment to SpyCage using plasmid pSL1515 and

161 pSL1510 respectively[43]. Plasmid DNA was purified (Qiagen HiSpeed Maxiprep Kit) precipitated
162 with ethanol, and resuspended in water before transfection using the Expi293 Expression
163 System (ThermoFisher, Expi293F cells, Expi293 Media, and the ExpiFectamine 293
164 Transfection Kit) by the Penn State Sartorius Cell Culture Facility as per manufacturer
165 instructions. Briefly, cells maintained in log phase growth at 37ºC and 8% CO2 in baffled flasks
166 shaking at 120-130 rpm were transfected at a concentration of 5 x 10^6/ml, and were
167 supplemented by the addition of ExpiFectamine 293 Transfection Enhancer 1 & 2 approximately
168 20 hours post-transfection. Culture supernatant was harvested by centrifugation (274 *xg*, 5
169 minutes, RT) on day three, and was incubated in batch with Ni-NTA (ThermoSci HisPur) resin
170 pre-equilibrated in 1xPBS at 4ºC for 1 hour on a nutator. The resin was then applied to a gravity
171 flow column and was washed four times with 10 column volumes of wash buffer (57 mM
172 NaH2PO4 pH 6.3@RT, 30 mM NaCl, 20 mM imidazole). Protein was eluted with 4 column
173 volumes of elution buffer (57 mM NaH2PO4 pH 7.9@RT, 30 mM NaCl, 235 mM imidazole).
174 Eluted protein was dialyzed to completion in 1xPBS and snap-frozen in liquid nitrogen for long-
175 term storage at -80ºC. Complete plasmid sequences are provided in Supp File 1.
176
177 ***Covalent Bonding of SARS-CoV-2 Spike RBD to SpyCage***
178 Purified SpyCage was dialyzed into 1xPBS with 1 mM DTT, and then mixed with purified SARS-
179 CoV-2 Spike RBD either with (RBD+SpyTag) or without (RBD only) at a 1.2:1 molar ratio of
180 RBD to SpyCage monomer in a buffer consisting of 1xPBS and 1mM DTT. The binding reaction
181 was allowed to go to completion by incubation for 3 hours at RT. The extent of SpyCage
182 saturation was assessed by SDS-PAGE as previously described[43]. The binding reaction was
183 then dialyzed into 1xPBS and stored at -80C until use in immunization efforts.
184
185 ***Cryo-EM specimen preparation and data collection***

186 Purified apo cage protein complex based upon I3-01[41,42] was first assessed by negative staining
187 to check sample quality and concentration before preparing TEM grids for data collection.
188 Briefly, a 3.5 ul aliquot was applied to a glow-discharged Cu-grid coated with a thin film of
189 continuous carbon, washed, stained with 0.75% w/v uranyl formate for 15 sec, blotted, air-dried,
190 and loaded on EFI Tecnai G2 Spirit BioTwin microscope (120 kV) for imaging.
191 TEM grids (QUANTAFOIL R2/1; QUANTAFOIL, Germany) were plasma cleaned using a
192 PELCO Glow Discharge System (Ted Pella, Redding CA). Aliquots of 3.5 ul of the apo cage
193 sample at approximately 0.1 mg/ml were applied to the grids, blotted for 2 sec, and then plunge-
194 frozen in liquid ethane using a vitrification robot (Vitrobot, Thermo Fisher). Grids were stored in
195 liquid nitrogen until the date of screening and data collection. Data was acquired on a Thermo
196 Fisher Titan Krios electron microscope (300 kV) equipped with Falcon 3EC direct detection
197 camera. EPU software (V 2.13.0.3175REL) was used to set up data acquisition at a nominal
198 magnification of x59,000 and a physical pixel size of 1.11 Å/pixel. A total of 1,220 micrographs
199 were recorded as movies (stacks of 39 frames) at an exposure rate of 1.15 e/Å^2/frame and a
200 total exposure time of 69.8 s. The nominal defocus range of -1.2 to -3.0 µm was applied during
201 data collection.
202
203 ***Cryo-EM Image processing***
204 Image analysis was performed using cryoSPARC software package (v3.3.2)[44]. Aligned movie
205 stacks were generated from raw micrographs after correcting for stage drift and anisotropic
206 motion using patch motion correction. Parameters of the contrast transfer function (CTF) were
207 estimated for each aligned movie in patch mode. Manually selected 283 particles from 11
208 micrographs were used to train a Topaz model for particle picking; a box of 420x420 pixel size
209 was used for particle extraction[45]. The trained model was applied to pick 129,792 particles from
210 1,202 micrographs. Further cleaning of the data using 2D classification resulted in 63,430
211 particles for subsequent data processing. A map from an *ab initio* model (generated using

212 10,000 particles) along with the selected clean particles were subjected to homogenous
213 refinement in cryoSPARC. Local motion correction[46] of the refined particles followed by
214 homogenous refinement with higher-order CTF terms enabled (including beam-tilt, spherical
215 aberration, trefoil and tetrafoil) and icosahedral symmetry (I1) enforced resulted in a final map at
216 3.4 Å resolution.
217
218 ***Cryo-EM Model building***
219 The initial model of the apo cage monomer was extracted from the published I3-01 model[41,42].
220 The monomer model was manually fitted into the 3.4 Å map in ChimeraX[47]; a full icosahedral
221 model of apo cage was generated from the asymmetric unit. PHENIX real-space refinement
222 was used to refine the model against the sharpened map with non-crystallographic symmetry
223 parameters applied[48]. The refined model was visually inspected in Coot and validated by
224 MolProbity[49,50]. All figures of the protein structure and cryo-EM map were created using
225 ChimeraX.
226
227 ***Culture of SARS-CoV-2***
228 The SARS-CoV-2/USA/WA1/2020 isolate was received from The World Reference Center for
229 Emerging Viruses and Arboviruses (WRCEVA), University of Texas Medical Branch at
230 Galveston (UTMB). The virus was obtained at passage 4 and was sub-cultured once on Vero
231 E6/TMPRSS2 cells (Japanese Collection of Research Bioresources Cell Bank). All titrations of
232 virus stocks and tissue homogenates were performed on Vero E6 cells (ATCC) cultured in
233 Dulbecco's modified Eagle Medium (Cytiva) supplemented with 10% FBS, 4 mM L-glutamine, 1
234 mM sodium pyruvate (Corning), 1X non-essential amino acids and 1X antibiotic and antimycotic
235 (Corning) at 37º C with 5% CO_2. For culture of the VeroE6/TMPRSS2 cells 1 mg/mL geneticin
236 was added to the media, and the FBS was reduced to 5%. To determine the titer of viral stocks,
237 the tissue culture infectious dose 50% (TCID50) was determined by inoculating cells grown in

238 24-well plates with serial dilutions of the virus. The plates were incubated at 37ºC with 5% CO_2
239 and scored for cytopathic effect at 96 hours post-infection. The $TCID_{50}$ was then calculated
240 using the method of Reed and Muench[51].
241
242 ***Vaccination and Challenge Experiments***
243 Equal numbers of male and female, six to eight-week-old Syrian hamsters (HsdHan:AURA,
244 Envigo, Haslett, MI) were used for all studies. After acclimatization, animals were implanted
245 with a subcutaneous transponder chip (Bio Medic Data Systems), and a pre-vaccination blood
246 sample was collected. For intranasal vaccination and virus inoculation, animals were sedated
247 and intranasally inoculated with a vaccine candidate (70 ul in 1xPBS) or SARS-CoV-2 (100 ul in
248 DMEM). For all experimental procedures, hamsters were sedated with 150 mg/kg ketamine, 7.5
249 mg/kg xylazine, and 0.015 mg/kg atropine via intraperitoneal injection. After completion of the
250 procedure, hamsters were given 1 mg/kg atipamezole subcutaneously. For tissue collection and
251 at the end of each study, hamsters were humanely euthanized via CO_2 asphyxiation.
252 *Trial 1: Evaluation of immunogenicity and efficacy of the SpyCage-RBD vaccine candidate*
253 To evaluate the immunogenicity and efficacy of the SpyCage RBD vaccine, groups of hamsters
254 (n=14/group) were intranasally vaccinated with PBS (mock), SpyCage (15 ug), SARS-CoV-2
255 RBD (10 ug), or SARS-CoV-2 RBD (10 ug) bound to SpyCage (15 ug, “RBD+SpyCage”).
256 Animals received a primary (1º) vaccination and a secondary (2º) vaccination 28 days later. The
257 vaccine was administered without adjuvants. Blood samples were collected via gingival vein
258 from 6 animals (3 males and 3 females) per group on days 14, 26, 42, and 55 post- 1º
259 vaccination. Blood samples were centrifuged at 1000 *x g* for 10 minutes at RT, and serum was
260 collected and stored at -20ºC. On day 56 post-1º vaccination, all animals were intranasally
261 inoculated with 10^5 $TCID_{50}$ SARS-CoV-2/USA/WA1/2020. On days 3 and 6 post-infection (day
262 59 and 62 post-1º vaccination), lung and nasal turbinate tissues were collected (n=4/group, 2

263 males and 2 females) and stored at -80ºC. The remaining six hamsters were monitored for
264 weight loss until day 14 (day 70 post-primary vaccination).
265 *Trial 2: Assessment of the requirement for grafting of RBD to SpyCage*
266 Groups of hamsters (n=18/group) were intranasally vaccinated with PBS (mock), SpyCage (15
267 ug), SARS-CoV-2 RBD (10 ug), SARS-CoV-2 RBD without SpyTag (10 ug) mixed with
268 SpyCage (15 ug) (*i.e.,* RBD could not covalently bond to SpyCage, "RBD|SpyCage"), and
269 SARS-CoV-2 RBD (10 ug) grafted to SpyCage (15 ug, "RBD+SpyCage"). The vaccination and
270 blood collection protocols were the same as in the initial study, and on day 56 post-1º
271 vaccination, animals were challenged with 1000 TCID50 of SARS-CoV-2. On days 3, 5, and 7
272 post-challenge (days 59, 61, and 63 post-primary vaccination), lung and nasal turbinates were
273 collected (n=4/group (2 males and 2 females)). One lung lobe was fixed with 10% v/v normal
274 buffered formalin and the remaining lung lobes and nasal turbinates were stored at -80ºC. The
275 remaining six hamsters/group were monitored for weight loss until day 14 post-SARS-CoV-2
276 challenge (day 70 post-primary vaccination). All animals were euthanized on day 15 post-
277 SARS-CoV-2 challenge.
278
279 ***Viral titration of tissue samples***
280 Collected lungs and nasal turbinates were homogenized in 2% FBS-DMEM containing 2X
281 antibiotic and antimycotic using an Omni tissue homogenizer. The homogenates were
282 centrifuged at 1000 *x g* for 10 minutes at 4ºC and the supernatant was titrated to determine the
283 tissue culture infectious dose 50% (TCID50) on Vero E6 cells as previously described[52].
284
285 ***Microneutralization Assay***
286 To determine titers of neutralizing antibodies, microneutralization assays were performed on
287 Vero E6 cells as previously described[52].
288

289 ***ELISA***

290 To assess the levels of RBD-binding IgG and IgA antibodies, ELISA assays were performed
291 according to a protocol generously provided by Dr. Sabra Klein, Johns Hopkins, School of
292 Public Health[53,54].

293

294 ***Histopathology***

295 Formalin-fixed lung samples were processed and stained with haematoxylin and eosin as
296 previously described[54]. Slides were scored by a board-certified veterinary pathologist using
297 established methods[55]. Each animal was scored for the extent of lesions (0-4), alveolar damage
298 (0- 3), bronchial damage (0-3), blood vessel damage (0-3), hemorrhage (0-2), and type II
299 pneumocyte hyperplasia (0-2). For each animal, a total pathology score was obtained by
300 calculating the sum of scores.

301

302 ***Biocontainment and Animal Care and Use***

303 All experiments using SARS-CoV-2 were conducted in an animal biosafety level 3 enhanced
304 laboratory. This facility is approved by the US Department of Agriculture and the Centers for
305 Disease Control and Prevention. All animal studies were conducted in compliance with the
306 Institutional Animal Care and Use Committee under protocol number 202001440.

307

308 ***Statistical Analysis***

309 Prism GraphPad (v9.0) was used to perform all statistical analyses with $p<0.05$ considered
310 significant. Weight loss and viral titers at each time point were evaluated for normality by
311 D'Agostino & Pearson test. For data sets that passed the normality test, one-way ANOVA with
312 post-hoc Tukey's test was performed. When data sets did not pass the normality test, Kruskal-
313 Wallis tests with a post-hoc Dunn's multiple comparison test were performed. Histopathological

314 scores were also compared using non-parametric Kruskal-Wallis tests with a post-hoc Dunn's
315 multiple comparison.
316
317 **RESULTS**
318 **Cryo-EM reconstruction and refinement of an atomic model of the apo cage scaffold**
319 To establish a robust, multimeric, spherical protein-based scaffold for intranasal immunizations
320 that would mimic the size of a viral particle, we selected a wireframe dodecahedron based upon
321 the previously described I3-01 protein, which was designed to self-assemble from 60
322 monomers[41,42]. To validate this scaffold structurally, we assessed a purified sample of this apo
323 cage complex by electron microscopy. Samples were first quality controlled by negative staining
324 with uranyl formate to assess particle integrity and concentration, and were then vitrified on gold
325 grids for cryo-EM data collection on our home-source Titan Krios electron microscope equipped
326 with a Falcon 3EC direct detection camera. Data processing and all aspects of the cryo-EM
327 workflow were conducted in cryoSPARC software (v.3.3.2)[44].
328
329 To create an experimentally determined high-resolution model, we collected a cryo-EM dataset
330 with 1,220 recorded movies to yield 1,202 processed micrographs with good-quality ice. These
331 were used to auto-pick and extract 129,792 particles using a box size of 420x420 pixels
332 (calibrated pixel size = 1.11 Å) (**Fig. 1A**, **Supplemental Table 1**). Then 2D classification was
333 used to clean up the data by removing junk particles (**Fig. 1B**) to produce a total of 63,430
334 particles for cryo-EM map reconstruction and refinement while imposing icosahedral symmetry.
335 The refinement produced a cryo-EM map at an average resolution of 3.4 Å and an estimated
336 local resolution in the range of 3.0 Å to 5.0 Å (**Fig. 1C**). Map resolution was determined based
337 on the gold-standard criterion that applies a Fourier Shell Correlation (FSC) cutoff value of
338 0.143 (**Fig. 1D**)[56]. The 3.4 Å resolution map showed the typical features of the designed apo
339 cage with an average diameter of 25 nm and the trimeric protein units occupying the vertices of

340 the pentameric faces of the dodecahedron. The I3-01 design PDB of this protein structure was
341 modified and used to initiate model building[41,42]. The map density was clear enough to build the
342 atomic structure using the published model of I3-01 to provide the starting coordinates. Real-
343 space refinement of the icosahedral model in PHENIX resulted in a 3.4 Å resolution model (**Fig.**
344 **1E**) with a cross-correlation value for model vs. map of 0.77 (CC masked, **Supplemental Table**
345 **1**). The geometrical parameters of the refined model checked by MolProbity revealed a good
346 quality model with a MolProbity score of 1.5, with approximately 98% of residues in the favored
347 region and no residues in the disallowed region of the Ramachandran plot. Quality-check
348 parameters of the model and map-model agreement are listed in **Supplemental Table 1**. The
349 3.4 Å resolution map showed clear density for most side chains of the amino acids constituting
350 the apo cage protein (aa 22-222) (**Fig. 1F)**. However, as expected for structures solved in the
351 range of 3.0 to 4.0 Å resolution[57], directionality of some carbonyl groups could not be resolved
352 unambiguously.
353 Comparing the solved cryo-EM structure and that from the computationally designed I3-01
354 model[41,42] showed that the two structures are almost identical [r.m.s. values of 0.57 Å for 200
355 Cα atoms and 1.29 Å for all non-hydrogen atoms], but the sidechain atoms of surface residues
356 had minor differences between our experimental and the computationally designed structures.
357
358 **Covalent Bonding of SARS-CoV-2 Spike RBD to SpyCage**
359 As the wireframe cage scaffold was robust, spherical, symmetrical, and could outwardly present
360 up to 60 fused proteins-of-interest, we selected it for further modification for antigen display.
361 Because the genetic fusion of antigens directly to protein-based scaffolds can influence
362 expression levels, solubility, and purification conditions needed, we leveraged the
363 SpyTag/SpyCatcher system to covalently link antigens-of-interest to the scaffold following its
364 purification[43]. This approach enables substantial versatility to load different proteins and their
365 variants without modifying the scaffold itself and has been used for a variety of viral and

366 parasitic pathogens to enhance immune responses[29-31,34-36,58]. To this end, we appended a
367 SpyCatcher domain with a flexible linker to the N-terminus of I3-01 so that all 60 subunits bear
368 this capture domain (schematic in **Fig. 2A**). We observed that this self-assembling scaffold
369 fused with SpyCatcher capture domains displayed excellent solubility and stability profiles when
370 expressed in *E. coli*, as it expressed to high levels and did not precipitate in standard laboratory
371 conditions (**Fig. 2B**). A comparable arrangement has been described for the mi3 variant of I3-
372 01, which also exhibited favorable display properties[30]. This scaffold, which we have termed
373 SpyCage, was advanced for all immunization studies presented here.
374 The use of SpyTag/SpyCatcher elements permits the versatile loading of antigens that are
375 independently expressed in an ideal expression system for that protein, thus ensuring that
376 proper post-translational modifications and processing events occur. Here, using 293F
377 suspension cells, we produced the receptor-binding domain (RBD) of SARS-CoV-2 Spike
378 protein with a C-terminal 6xHis tag, and either with or without an additional C-terminal SpyTag
379 (**Fig. 2A**). Secreted protein was purified from the culture supernatant to >99% purity via Ni-NTA
380 affinity chromatography (**Fig. 2B**). Mixing of SpyCage with RBD ("RBD+SpyCage")at a 1 to 1.2
381 molar ratio in 1xPBS led to the formation of a covalent bond that could be detected by a mobility
382 shift by SDS-PAGE with >95% saturation of the scaffold with RBD (**Fig. 2B**). This molar ratio
383 consistently achieves this maximal degree of saturation for RBD and other comparably sized,
384 globular antigens (data not shown). In contrast, when SpyCage was mixed with RBD lacking a
385 SpyTag ("RBD|SpyCage"), no covalent linkage formed between the RBD and SpyCage, as
386 intended (**Fig. 2B**). This second combination creates an admixture ("RBD|SpyCage") that
387 permits testing of the effect that covalent bonding of the antigen to the scaffold has upon
388 efficacy. From this we concluded that SpyCage is a stable and saturable antigen display
389 platform capable of presenting antigens-of-interest in a versatile mix-and-go format. As
390 SpyCage has similar structural properties as a virus particle and displays 5-15 copies of an
391 antigen on a single face of the scaffold (up to a total of 60 antigens per particle), we

392 hypothesized SpyCage grafted with RBD would be a greatly improved vaccine candidate. As
393 there is an urgent need for the development of vaccines inducing mucosal immunity, we
394 proceeded to evaluate SpyCage as an intranasal vaccine.
395
396 **RBD grafting to SpyCage is required to induce an antibody response**.
397 To assess the immunogenicity of RBD+SpyCage as an intranasal vaccine candidate (*i.e.,* Trial
398 1), hamsters were given a 1º and 2º intranasal vaccine consisting of PBS (mock), SpyCage,
399 RBD, or RBD+SpyCage. The two vaccine doses were administered 28 days apart and the
400 vaccines were formulated without adjuvants. Serum samples were collected prior to each
401 vaccination and the day before viral challenge. To assess the antibody response, levels of RBD-
402 binding IgG antibodies in the serum were quantified by ELISA and neutralizing antibodies were
403 assayed by a microneutralization assay. We found that only the RBD+SpyCage vaccinated
404 animals developed an IgG antibody response (**Fig. S1A**). On day 28, one animal had IgG
405 antibodies against RBD, while on day 55, 4/6 animals given RBD+SpyCage developed an
406 antibody response (**Fig. S1A)**; however, while these antibodies were able to bind RBD, they did
407 not exhibit neutralizing activity (**Fig. S1B**).
408 Subsequently, we conducted an expanded vaccine study (designated Trial 2) to determine if
409 grafting of RBD directly to SpyCage through covalent bonding was required to induce an
410 antibody response. Animals were vaccinated according to the same regimen; however, an
411 additional group in which RBD without SpyTag was mixed with SpyCage ("RBD|SpyCage") was
412 included to test the importance of the bonding of RBD to SpyCage. Therefore, the experimental
413 groups consisted of animals given the following vaccines: 1) Mock (PBS), 2) RBD, 3) SpyCage,
414 4) RBD mixed with but not bound to SpyCage (RBD|SpyCage), and 5) RBD grafted to SpyCage
415 (RBD+SpyCage). In both vaccination studies, animals were monitored for 7 days post-1º and 2º
416 vaccination for adverse effects. None of the animals exhibited weight loss or clinical signs,
417 indicating the vaccine was well-tolerated (data not shown).

418 Evaluation of the antibody response by ELISA and microneutralization assay (**Fig. 3**) showed
419 that none of the mock, SpyCage, RBD alone, or RBD|SpyCage immunized animals developed
420 RBD-directed antibodies on day 28 or 55. In contrast, animals vaccinated with RBD+SpyCage
421 developed IgG antibodies against RBD on day 28 post-1º vaccination (2/6 animals positive) and
422 on day 55 (5/6 animals positive) (**Fig. 3A**). While most animals in the RBD+SpyCage group
423 developed IgG antibodies by day 55, only one animal developed an IgA antibody response (**Fig.**
424 **3B**). This was one of the two animals that developed IgG antibodies early (day 28) and was the
425 animal with the highest IgG antibody titer on day 55 (1: 12800) (**Fig. 3A**). In addition, the serum
426 from this animal exhibited neutralizing activity (**Fig. 3C**), while none of the other animals
427 developed a neutralizing antibody response. Thus, while we did not observe 100%
428 seroconversion, the RBD+SpyCage vaccine candidate was reproducibly capable of inducing
429 IgG antibodies. As one animal developed both a neutralizing antibody response and IgA
430 antibodies indicative of mucosal immunity, our findings indicate that, with additional
431 modifications to enhance immunogenicity, intranasal vaccination with RBD+SpyCage could
432 induce mucosal immunity. Furthermore, these findings demonstrate the RBD+SpyCage vaccine
433 provides a substantial boost in antibody responses compared to RBD alone or an
434 RBD|SpyCage admixture where the covalent bond needed for grafting cannot form.
435 To address the immunogenicity of SpyCage itself, we also evaluated the antibody response to
436 SpyCage by ELISA (**Fig. 3D)**. All animals given a vaccine containing SpyCage developed IgG
437 antibodies directed towards the scaffold. While there were no statistically significant differences
438 between different vaccine groups that received the SpyCage, the RBD|SpyCage admixture
439 increased the antibody response 2-fold compared to animals given SpyCage alone, and
440 RBD+SpyCage further increased the response by 2-fold (*i.e.,* 4-fold relative to SpyCage alone).
441 These findings indicate that grafting the antigen to SpyCage enhances the antibody response to
442 both the scaffold and the antigen.
443

444 **Intranasal vaccination with RBD+SpyCage enhances clearance of SARS-CoV-2 from the**
445 **respiratory tract**
446 To assess the efficacy of the RBD+SpyCage vaccine candidate, in both vaccine trials of this
447 study, we assessed whether RBD+SpyCage enhanced viral clearance and reduced clinical
448 illness. In the second trial, we also evaluated the effect of vaccination on reducing lung
449 pathology. In Trial 1, vaccinated hamsters were challenged with 10^5 TCID50 SARS-CoV-2 on
450 day 56 post-1º vaccination (day 28 post-2º vaccination). After viral challenge, animals were
451 monitored for weight loss for 14 days, and on days 3 and 5 post-infection (p.i.), lung and nasal
452 turbinate samples were collected from a subset of animals (n=4/group/timepoint) (**Fig. S2**).
453 After viral challenge, animals in all experimental groups lost weight (**Fig. S2A**) and there were
454 no statistically significant differences between the groups; however, the animals that received
455 RBD+SpyCage had reduced weight loss, and by the end of the study, these animals exceeded
456 their pre-challenge weight. When we evaluated viral titers in the lungs and nasal turbinates, on
457 day 3 p.i. all experimental groups had high titers of replicating virus in these tissues with no
458 significant differences between groups. On day 6 p.i., viral titers in both tissues were reduced
459 for all groups; however, while the mock and SpyCage-vaccinated animals had replicating virus
460 in the nose and lungs, no replicating virus was recovered from the RBD only and
461 RBD+SpyCage vaccinated animals (**Fig. S2 B,C**). These findings suggested vaccination with
462 RBD or RBD+SpyCage facilitated viral clearance.
463 While vaccination with either RBD only or RBD+SpyCage reduced viral load on day 6, only the
464 RBD+SpyCage vaccinated animals developed an IgG antibody response. We therefore
465 performed a second, expanded vaccination study (i.e., Trial 2) to evaluate if grafting of RBD to
466 SpyCage via covalent bonding was required for protection. Here we repeated the vaccination
467 study with an additional group of animals that were vaccinated with an admixture of RBD and
468 SpyCage where the covalent bond needed for grafting could not form (RBD|SpyCage). As the
469 10^5 $TCID_{50}$ challenge dose used in the initial study is 2-3 orders of magnitude higher than the

470 estimated infectious dose for humans (*i.e.,* 100-1000 infectious units)[59,60], we reduced the
471 challenge dose to 1000 TCID50 of SARS-CoV-2. This challenge dose was previously shown to
472 induce weight loss in hamsters[61], which we also verified with our virus stock (**Fig. S3)**. Finally,
473 to evaluate the dynamics of viral clearance more comprehensively, we also modified the time
474 points of tissue collection such that tissues were collected on days 3, 5, and 7 p.i.
475 After viral challenge, the animals in all experimental groups lost weight, with peak weight-loss at
476 day 6 or 7. However, while there were no statistically significant differences in weight loss
477 between experimental groups (**Fig. 4A**), consistent with our first study, we also observed that
478 animals vaccinated with RBD+SpyCage trended toward reduced weight loss compared to the
479 other groups (**Fig. 4A**). We next evaluated viral replication in the nasal turbinates and lungs.
480 On day 3 p.i., mean viral load in the nasal turbinates and lungs for all groups were comparable,
481 with titers greater than 10^5 and 10^6 TCID50/gm in each tissue, respectively (**Fig. 4 B,C**).
482 However, on day 5 p.i. the mean viral titer in the nasal turbinates for the RBD+SpyCage group
483 was significantly lower (25 TCID50/gm) compared to the other experimental groups (titer range:
484 881 – 3955 TCID50/gm) (**Fig. 4B**). Similarly, in the lungs, RBD+SpyCage vaccinated animals
485 also had significantly lower titers (1183 TCID50/gm) (titer range for other experimental
486 groups:11,988 – 59,356 TCID50/gm) (**Fig. 4C**). On day 7 p.i., replicating virus was not detected
487 in the nasal turbinates or lungs from any of the experimental groups (**Fig. 4 B,C**). Therefore,
488 while viral titers on days 3 and 7 in the nasal turbinates and lungs were comparable for all
489 groups, on day 5 viral titers in the RBD+SpyCage vaccinated animals were more than 10-fold
490 lower, indicating that the RBD+SpyCage vaccinated animals more rapidly cleared SARS-CoV-2
491 from both the upper and lower respiratory tract.
492 Last, we performed a histopathology analysis to determine if the RBD+SpyCage vaccinated
493 animals had reduced lung inflammation and damage. Lung tissue sections were blinded and
494 scored for the extent of lesions, alveolar, bronchial, and blood vessel damage, as well as
495 hemorrhage and type II pneumocyte hyperplasia. These scores were then combined to give a

total pathology score. Representative images of lung pathology and inflammation from each group are shown in **Fig. 5A.** The largest differences in pathology scores were observed in the total pathology score and the extent of lesions (**Fig. 5 B,C)**, with additional scores reported in **Fig. S4**. On day 3, all groups exhibited similar pathology. For the mock vaccinated animals, the total pathology score and extent of lesions peaked on day 5 and then declined on day 7. The RBD+SpyCage vaccinated animals exhibited the lowest total pathology and extent of lesions scores compared to all other groups on both days 5 and 7. Animals receiving SpyCage, RBD, or the SpyCage|RBD admixture had intermediate scores between the mock and SpyCage+RBD groups on day 5, and had pathology scores comparable to mock infected animals on day 7. While the pathology scoring shows a trend towards reduced pathology with the SpyCage+RBD group, this difference was not statistically significant due to the limited number of animals used at each time point. Future studies can leverage these observed effect sizes to establish expanded group sizes to determine if these promising trends are maintained.

509 **DISCUSSION**

510 The development of efficacious intranasal vaccines has the potential to prevent SARS-CoV-2
511 infections and reduce transmission[62]. To date several pre-clinical intranasal vaccine candidates
512 have been developed [63]; however, most candidates are live-attenuated or viral vector vaccines.
513 Due to safety concerns, the administration of these vaccines is often limited to healthy adults
514 (18-55 years old) and/or older children. In contrast, recombinant protein or inactivated vaccines
515 are widely used in individuals of all ages. Therefore, we sought to develop a recombinant
516 protein-based intranasal vaccine.

517 Because immune responses can be enhanced when antigens-of-interest are displayed on a
518 scaffold, we established design criteria for an intranasal vaccine candidate. These criteria
519 included 1) rigid bodies, 2) a spherical shape of ~20-30 nm in diameter, and 3) genetically
520 accessible N- and/or C-termini presented in an outward-facing manner. I3-01 met all these
521 criteria and was selected as the strongest candidate. To date, only a lower resolution cryo-EM
522 reconstruction and a computational model of I3-01 have been published[41]. Therefore, we used
523 both negative stain TEM and cryo-EM to resolve the I3-01-based scaffold (apo cage) to a 3.4A
524 average resolution and validated that the experimentally derived atomic model closely matched
525 the computationally designed protein (**Fig. 1**). We then proceeded with using I3-01 to create
526 SpyCage by further modifying I3-01 to bear an N-terminal SpyCatcher domain with a 12 amino
527 acid flexible linker to reduce steric hindrance and permit greater saturation of antigens. As
528 anticipated, the SpyTag/SpyCatcher system enabled rapid, covalent linkage of RBD to SpyCage
529 (RBD+SpyCage) to near saturation as seen by a mobility shift by SDS-PAGE (**Fig. 2**).
530 Importantly, the RBD+SpyCage preparation remained highly soluble and stable over time, which
531 further supports its feasibility as a vaccine candidate.

532 Subsequently, we assessed the immunogenicity of the RBD+SpyCage vaccine in the gold
533 standard Syrian hamster model (*i.e.,* Trial 1). Animals were given an unadjuvanted prime-boost

534 intranasal vaccination 28 days apart, and then challenged 28 days later (day 56 post-primary
535 vaccination) with SARS-CoV-2. On day 26 post-primary vaccination, 1 of 6 RBD+SpyCage
536 vaccinated hamsters developed serum IgG antibodies, and by day 55, most animals (4/6) had a
537 measurable IgG response. None of the animals developed neutralizing antibodies (**Fig. S1**).
538 Following viral challenge, all animals, regardless of vaccination status, lost weight, although
539 there was a trend towards reduced weight loss and earlier recovery in the RBD+SpyCage
540 vaccinated animals (**Fig. S2**). Based on these outcomes, we next sought to determine the
541 properties of the vaccine that enhanced immunogenicity.

542 Studies on intramuscular vaccination have shown that presenting viral antigens on the surface
543 of particles enhances the immune presentation and protective efficacy of vaccines[64]. Therefore,
544 we expanded upon our initial study and compared RBD+SpyCage (in which RBD is covalently
545 bound to the scaffold) to an RBD|SpyCage admixture lacking this covalent attachment. Covalent
546 grafting was shown to be a requirement for immunogenicity, as 2/6 and 5/6 animals given
547 RBD+SpyCage developed an IgG response on days 28 and 55, respectively against RBD (**Fig**
548 **3**). The one animal that exhibited the highest IgG titers on day 28 and day 55, also developed
549 an IgA response, and these antibodies exhibited neutralizing activity. In contrast, animals
550 vaccinated with RBD|SpyCage (*i.e.,* RBD mixed with, but not covalently bound to SpyCage) did
551 not develop an antibody response to RBD. Further studies are warranted to explore strategies
552 to enhance the immunogenicity of RBD+SpyCage to match the neutralizing IgG and IgA
553 response we observed in this one animal.

554 As a final component of our antibody analyses, we evaluated the response generated against
555 the SpyCage scaffold. All animals that received SpyCage as a component of the vaccine
556 developed antibodies directed towards the scaffold. Our results do not suggest this immunity
557 interfered with the immune response to RBD, as boost vaccination increased the response to
558 RBD. However, in future studies, if immunity against the scaffold interferes with immunogenicity

559 for other vaccine antigens, alternative scaffolds can be evaluated for subsequent intranasal
560 vaccinations[65]. Importantly, assessment of the immune response in hamsters is currently
561 hampered by a limited number of species-specific reagents. Reagents to assess mucosal and
562 cellular immunity are lacking. Using our existing protocol, we previously performed ELISA on
563 matched convalescent hamster serum and nasal wash samples[54]. While we detected serum IgA
564 antibodies, we could not detect antibodies in the nasal wash (data not shown). Therefore, as
565 new reagents are developed for hamsters, it will be important to expand the immunological
566 assessment of vaccine responses.

567 Covalent grafting to SpyCage was also a requirement for vaccine efficacy. Upon SARS-CoV-2
568 challenge in Trial 2, all animals lost weight; however, compared to the other groups,
569 RBD+SpyCage vaccinated animals had a trend towards reduced weight loss and reduced lung
570 pathology. This was associated with significantly reduced levels of replicating virus in the
571 respiratory tract on day 5, indicating rapid viral clearance in the RBD+SpyCage group relative to
572 the RBD|SpyCage group **(Fig 4)**. Future studies could pinpoint a more comprehensive view of
573 the dynamics and changes in viral clearance. Collectively, the induction of non-neutralizing
574 RBD-binding antibodies in association with accelerated viral clearance and trends towards
575 reduced disease severity and pathology suggests alternative antibody-mediated mechanisms
576 (*e.g.,* antibody-dependent cell-mediated cytotoxicity (ADCC) or antibody-dependent cellular
577 phagocytosis (ADCP)), and/or that T cell mediated immunity contributed to protection.
578 To our knowledge, this is the first report of a scaffolded antigen being used as an intranasal
579 protein-based vaccine. Other groups have used the I3-01 scaffold successfully as a vaccine
580 platform to display antigens for influenza, SARS-CoV-2, and *Plasmodium*, but have only
581 explored intramuscular administration[30,37,58,66-69]. Several groups have expressed the RBD or S-
582 protein on I3-01 and evaluated the immunogenicity of these scaffolded antigens as
583 intramuscular vaccines in animal models[37,58,66-68]. In these studies, the vaccine candidates were

584 administered with an adjuvant (*e.g.,* Addavax, Alum, CpG), and potent neutralizing antibody
585 responses were induced in mice, hamsters, pigs, or non-human primates[37,58,66-68]. Given both
586 the route of administration and the inclusion of adjuvants, this is the expected antibody
587 response. In comparison, we administered the RBD+SpyCage vaccine only via the intranasal
588 route and without an adjuvant, which induced a non-neutralizing IgG antibody response.
589 Prior studies have evaluated the protective efficacy of intramuscular vaccination with RBD
590 grafted to I3-01 against SARS-CoV-2 challenge[37,58]. When hamsters were intramuscularly
591 vaccinated and challenged with SARS-CoV-2, consistent with our results, all animals lost
592 weight, and the RBD-I3-01 vaccinated animals (designated "RBD-VLP" in that study) had
593 reduced weight loss relative to animals vaccinated with RBD alone[37]. Unfortunately, in this
594 study, viral titers were not evaluated in lung or nasal turbinate samples after viral infection,
595 precluding a comparison with our findings. In another study, when transgenic K18-hACE2 mice
596 were vaccinated with a similar construct, SARS-CoV-2 Beta RBD-mi3, and challenged, all
597 vaccinated mice survived a lethal challenge while only 20% of control animals survived. In
598 parallel, with enhanced survival, no replicating virus was detected in the lungs of the RBD-mi3
599 vaccinated animals[58]. Similarly, when Rhesus macaques were vaccinated with the same
600 construct and challenged with SARS-CoV-2, at both day 2 and 4 p.i. significantly lower titers of
601 virus were detected in nasal swabs compared to unimmunized controls. Moreover, in RBD-mi3
602 vaccinated animals, replicating virus was not recovered from bronchioloalveolar lavage fluids
603 (BAL) (i.e., 0/4), while 3/4 unimmunized controls had between 10^3 – 10^6 TCID50/mL of SARS-
604 CoV-2 in the BAL[58]. In addition to I3-01, the bipartite I53-50 icosahedral scaffold consisting of
605 120-subunit proteins has also been decorated with either the RBD or S-protein and utilized as
606 an intramuscular vaccine[29,70]. Consistent with intramuscular vaccination with I3-01,
607 intramuscular vaccination with RBD or S-protein grafted to I53-50 combined with an adjuvant
608 induced a neutralizing antibody response in mice, rabbits, or macaques [29,70]. In these studies,
609 only macaques vaccinated with S-protein on I53-50 nanoparticles were challenged with SARS-

610 CoV-2. Following viral challenge, relative to unimmunized controls, vaccinated animals had
611 reduced clinical manifestations associated with significantly reduced viral titers in the upper
612 airways and BAL from day 1 until resolution on day 7 p.i.[29]. In contrast to these studies, when
613 we challenged the RBD+SpyCage vaccinated animals, we did not observe an initial reduction in
614 SARS-CoV-2 replication as all animals had similar titers on day 3 p.i.; however, the
615 RBD+SpyCage vaccinated animals had reduced titers on day 5 indicating accelerated viral
616 clearance. We also observed trends towards reduced weight loss and reduced pathology;
617 however, these were not statistically significant. The reduced efficacy observed in our studies
618 relative to intramuscular vaccination is most likely due to a lack of a neutralizing antibody
619 response following intranasal vaccination. In our studies, we purposefully did not include an
620 adjuvant as there are no licensed intranasal adjuvants for human use; however, future
621 development of the intranasal RBD+SpyCage vaccine warrants the inclusion of intranasal
622 adjuvants to enhance the quality of the antibody response and vaccine efficacy. In addition, to
623 more closely model immunity in the human population, a recent study explored intranasal
624 vaccination with recombinant S-protein as a booster in animals previously given intramuscular
625 vaccines[71]. This approach enhanced protection, and based on our findings, we posit that such
626 an intranasal boost would benefit from scaffolding the S-protein or its derivatives.
627 Collectively, we demonstrate intranasal vaccination with RBD grafted to SpyCage induced a
628 serum IgG response in hamsters. Upon viral challenge, this response was associated with
629 enhanced viral clearance from both the upper and lower respiratory tract. RBD+SpyCage
630 vaccinated animals also exhibited non-significant reductions in weight loss and lung pathology
631 consistent with a non-neutralizing antibody response. We further show the immunogenicity and
632 efficacy of the RBD+SpyCage vaccine required that RBD was covalently linked to the SpyCage
633 scaffold. These studies demonstrate the potential for intranasal delivery of SpyCage scaffolded
634 antigens as a vaccine platform, and additional vaccine development is warranted with the
635 inclusion of intranasal adjuvants to enhance immunogenicity. Moreover, given the relative ease

636 with which vaccine antigens can be grafted to the scaffold and the potential to induce mucosal
637 immunity, SpyCage-derived intranasal vaccines can be developed to target other respiratory
638 viruses, and if successful, this platform could also be used as a rapid response vaccine platform
639 to target novel or pandemic pathogens.

640 **DATA AVAILABILITY**

641 The icosahedral map of the solved apo cage structure is deposited in EM data bank under
642 accession code EMD-27812. The apo cage atomic model is deposited in the PDB data bank
643 under ID 8E01. A validation report is provided as Supp File 2 for peer review purposes.

644

645 **ACKNOWLEDGMENTS**

646 SH, SEL, and TCS planned all experiments with assistance from DRP and AM. AM and SEL
647 designed and purified recombinant proteins and vaccine candidates. RMR expressed the RBD
648 protein. All cryo-EM studies were conducted by CB, IMM, and SH. Vaccination and challenge
649 studies were conducted by DRP with assistance from DGS, CJF, AK, and TH. EHL performed
650 histopathology and analysis of lung samples. DRP, SH, SEL and TCS prepared the final
651 manuscript.
652 The molecular graphics and analyses were performed with UCSF ChimeraX, developed by the
653 Resource for Biocomputing, Visualization, and Informatics at the University of California, San
654 Francisco, with support from National Institutes of Health R01-GM129325 and the Office of
655 Cyber Infrastructure and Computational Biology, National Institute of Allergy and Infectious
656 Diseases. We would like to acknowledge Dr. David Baker from the University of Washington for
657 providing I3-01_HisR4 plasmid, Dr. Florian Krammer from Mount Sinai School of Medicine, for
658 providing the pCAGGS plasmid for SARS-CoV-2 Spike RBD expression, and Dr. Sabra Klein,
659 Johns Hopkins, School of Public Health for generously providing the IgG and IgA ELISA
660 protocols. We also acknowledge Bob Ashley at Penn State College of Medicine for pilot electron
661 microscopy efforts. Lastly, we would also like to acknowledge the Sartorius Huck Cell Culture
662 Facility for early access and production of SARS-CoV-2 Spike RBD protein.

663 **FUNDING**

664 The design and expression of the SpyCage scaffold was conducted by SEL and SH under
665 NIGMS R01GM125907. Seed Grant funding to SEL and TCS from the Pennsylvania State
666 University Huck Institutes of Life Sciences supported the vaccination and challenge studies.
667 Funding for TCS was also provided by the USDA National Institute of Food and Agriculture,
668 Hatch project 4771.

669

670 **DISCLOSURES**

671 We wish to disclose the following intellectual property claims related to this study:

672 **Lindner, S.E.** & **Hafenstein, S.** US Patent Application 16/494,502 "Versatile Display for
673 Proteins"

674 **Lindner, S.E.**, **Hafenstein, S.**, & Butler, N. PCT/US2020/033785 "Specific Selection of Immune
675 Cells Using Versatile Display Scaffolds"

676 **Lindner, S.E.**, **Sutton, T.C.**, **Hafenstein, S.**, & Butler, N. US Trademark Application 9063755
677 "SPYCAGE"

678 **REFERENCES**

679

680 1 Zhu, N. *et al.* A Novel Coronavirus from Patients with Pneumonia in China, 2019. *New*
681 *England Journal of Medicine* **382**, 727-733, doi:10.1056/nejmoa2001017 (2020).
682 2 Kadam, S. B., Sukhramani, G. S., Bishnoi, P., Pable, A. A. & Barvkar, V. T. SARS-CoV-
683 2, the pandemic coronavirus: Molecular and structural insights. *Journal of Basic*
684 *Microbiology* **61**, 180-202, doi:10.1002/jobm.202000537 (2021).
685 3 Fehr, A. R. & Perlman, S. in *Coronaviruses* 1-23 (Springer New York, 2015).
686 4 Premkumar, L. *et al.* The receptor-binding domain of the viral spike protein is an
687 immunodominant and highly specific target of antibodies in SARS-CoV-2 patients.
688 doi:10.1126/sciimmunol.abc8413 (2020).
689 5 Piccoli, L. *et al.* Mapping Neutralizing and Immunodominant Sites on the SARS-CoV-2
690 Spike Receptor-Binding Domain by Structure-Guided High-Resolution Serology. *Cell*
691 **183**, 1024-1042.e1021, doi:10.1016/j.cell.2020.09.037 (2020).
692 6 Krammer, F. SARS-CoV-2 vaccines in development. *Nature* **586**, 516-527,
693 doi:10.1038/s41586-020-2798-3 (2020).
694 7 Organization, W. H. *COVID-19 vaccine tracker and landscape*, <COVID-19 vaccine
695 tracker and landscape (who.int)> (
696 8 *COVID-19 Vaccines: The full list*, <https://covidvax.org> (2022).
697 9 Z, W. *et al.* Safety, tolerability, and immunogenicity of an inactivated SARS-CoV-2
698 vaccine (CoronaVac) in healthy adults aged 60 years and older: a randomised, double-
699 blind, placebo-controlled, phase 1/2 clinical trial. *The Lancet. Infectious diseases* **21**,
700 doi:10.1016/S1473-3099(20)30987-7 (2021).
701 10 Y, Z. *et al.* Safety, tolerability, and immunogenicity of an inactivated SARS-CoV-2
702 vaccine in healthy adults aged 18-59 years: a randomised, double-blind, placebo-

703 controlled, phase 1/2 clinical trial. *The Lancet. Infectious diseases* **21**,
704 doi:10.1016/S1473-3099(20)30843-4 (2021).
705 11 K, Z. *et al.* Safety and immunogenicity of a QazCovid-in® inactivated whole-virion
706 vaccine against COVID-19 in healthy adults: A single-centre, randomised, single-blind,
707 placebo-controlled phase 1 and an open-label phase 2 clinical trials with a 6 months
708 follow-up in Kazakhstan. *EClinicalMedicine* **39**, doi:10.1016/j.eclinm.2021.101078
709 (2021).
710 12 S, X. *et al.* Effect of an Inactivated Vaccine Against SARS-CoV-2 on Safety and
711 Immunogenicity Outcomes: Interim Analysis of 2 Randomized Clinical Trials. *JAMA* **324**,
712 doi:10.1001/jama.2020.15543 (2020).
713 13 N, A. K. *et al.* Effect of 2 Inactivated SARS-CoV-2 Vaccines on Symptomatic COVID-19
714 Infection in Adults: A Randomized Clinical Trial. *JAMA* **326**, doi:10.1001/jama.2021.8565
715 (2021).
716 14 Xia, X. Detailed Dissection and Critical Evaluation of the Pfizer/BioNTech and Moderna
717 mRNA Vaccines. *Vaccines* **9**, 734, doi:10.3390/vaccines9070734 (2021).
718 15 Creech, C. B., Walker, S. C. & Samuels, R. J. SARS-CoV-2 Vaccines. *JAMA* **325**, 1318,
719 doi:10.1001/jama.2021.3199 (2021).
720 16 Machhi, J. *et al.* Nanocarrier vaccines for SARS-CoV-2. *Advanced Drug Delivery*
721 *Reviews* **171**, 215-239, doi:10.1016/j.addr.2021.01.002 (2021).
722 17 Study of the Safety, Reactogenicity and Immunogenicity of "EpiVacCorona" Vaccine for
723 the Prevention of COVID-19 - Full Text View - ClinicalTrials.gov. (2022).
724 18 VP, C., LK, V., AK, P. & VB, P. Intranasal vaccines for SARS-CoV-2: From challenges to
725 potential in COVID-19 management. *Drug discovery today* **26**,
726 doi:10.1016/j.drudis.2021.07.021 (2021).
727 19 Yusuf, H. & Kett, V. Current prospects and future challenges for nasal vaccine delivery.
728 *Hum Vaccin Immunother* **13**, 34-45, doi:10.1080/21645515.2016.1239668 (2017).

20 Chemaitelly, H. *et al.* Waning of BNT162b2 Vaccine Protection against SARS-CoV-2 Infection in Qatar. *New England Journal of Medicine* **385**, e83, doi:10.1056/nejmoa2114114 (2021).

21 Keehner, J. *et al.* Resurgence of SARS-CoV-2 Infection in a Highly Vaccinated Health System Workforce. *New England Journal of Medicine* **385**, 1330-1332, doi:10.1056/nejmc2112981 (2021).

22 RWY, C. *et al.* The Mucosal and Serological Immune Responses to the Novel Coronavirus (SARS-CoV-2) Vaccines. *Frontiers in immunology* **12**, doi:10.3389/fimmu.2021.744887 (2021).

23 Hajnik, R. L. *et al.* Dual spike and nucleocapsid mRNA vaccination confer protection against SARS-CoV-2 Omicron and Delta variants in preclinical models. *Sci Transl Med* **14**, eabq1945, doi:10.1126/scitranslmed.abq1945 (2022).

24 Lund, F. E. & Randall, T. D. Scent of a vaccine. *Science* **373**, 397-399, doi:10.1126/science.abg9857 (2021).

25 Topol, E. J. & Iwasaki, A. Operation Nasal Vaccine-Lightning speed to counter COVID-19. *Sci Immunol*, eadd9947, doi:10.1126/sciimmunol.add9947 (2022).

26 WHO, W. H. O. *The Oxford/AstraZeneca (ChAdOx1-S [recombinant] vaccine) COVID-19 vaccine: what you need to know*, <https://www.who.int/news-room/feature-stories/detail/the-oxford-astrazeneca-covid-19-vaccine-what-you-need-to-know> (2022).

27 FDA, U. F. a. D. A. *Coronavirus (COVID-19) Update: FDA Limits Use of Janssen COVID-19 Vaccine to Certain Individuals*, <https://www.fda.gov/news-events/press-announcements/coronavirus-covid-19-update-fda-limits-use-janssen-covid-19-vaccine-certain-individuals> (2022).

28 Sridhar, S., Brokstad, K. A. & Cox, R. J. Influenza Vaccination Strategies: Comparing Inactivated and Live Attenuated Influenza Vaccines. *Vaccines (Basel)* **3**, 373-389, doi:10.3390/vaccines3020373 (2015).

755 29 Brouwer, P. J. M. *et al.* Two-component spike nanoparticle vaccine protects macaques
756 from SARS-CoV-2 infection. *Cell* **184**, 1188-1200 e1119, doi:10.1016/j.cell.2021.01.035
757 (2021).
758 30 Bruun, T. U. J., Andersson, A. C., Draper, S. J. & Howarth, M. Engineering a Rugged
759 Nanoscaffold To Enhance Plug-and-Display Vaccination. *ACS Nano* **12**, 8855-8866,
760 doi:10.1021/acsnano.8b02805 (2018).
761 31 Caradonna, T. M. & Schmidt, A. G. Protein engineering strategies for rational
762 immunogen design. *NPJ Vaccines* **6**, 154, doi:10.1038/s41541-021-00417-1 (2021).
763 32 Cohen, A. A. *et al.* Mosaic nanoparticles elicit cross-reactive immune responses to
764 zoonotic coronaviruses in mice. *Science* **371**, 735-741, doi:10.1126/science.abf6840
765 (2021).
766 33 Hsieh, C. L. & McLellan, J. S. Protein engineering responses to the COVID-19
767 pandemic. *Curr Opin Struct Biol* **74**, 102385, doi:10.1016/j.sbi.2022.102385 (2022).
768 34 Liu, Z. H. *et al.* Self-Assembling Nanovaccine Enhances Protective Efficacy Against
769 CSFV in Pigs. *Front Immunol* **12**, 689187, doi:10.3389/fimmu.2021.689187 (2021).
770 35 Malhi, H. *et al.* Immunization with a self-assembling nanoparticle vaccine displaying EBV
771 gH/gL protects humanized mice against lethal viral challenge. *Cell Rep Med* **3**, 100658,
772 doi:10.1016/j.xcrm.2022.100658 (2022).
773 36 Nguyen, B. & Tolia, N. H. Protein-based antigen presentation platforms for nanoparticle
774 vaccines. *NPJ Vaccines* **6**, 70, doi:10.1038/s41541-021-00330-7 (2021).
775 37 Dalvie, N. C. *et al.* Engineered SARS-CoV-2 receptor binding domain improves
776 manufacturability in yeast and immunogenicity in mice. *Proc Natl Acad Sci U S A* **118**,
777 doi:10.1073/pnas.2106845118 (2021).
778 38 Chan, J. F. *et al.* Simulation of the Clinical and Pathological Manifestations of
779 Coronavirus Disease 2019 (COVID-19) in a Golden Syrian Hamster Model: Implications

780 for Disease Pathogenesis and Transmissibility. *Clin Infect Dis* **71**, 2428-2446,
781 doi:10.1093/cid/ciaa325 (2020).
782 39 Imai, M. *et al.* Syrian hamsters as a small animal model for SARS-CoV-2 infection and
783 countermeasure development. *Proc Natl Acad Sci U S A* **117**, 16587-16595,
784 doi:10.1073/pnas.2009799117 (2020).
785 40 Rosenke, K. *et al.* Defining the Syrian hamster as a highly susceptible preclinical model
786 for SARS-CoV-2 infection. *Emerg Microbes Infect* **9**, 2673-2684,
787 doi:10.1080/22221751.2020.1858177 (2020).
788 41 Hsia, Y. *et al.* Design of a hyperstable 60-subunit protein dodecahedron. [corrected].
789 *Nature* **535**, 136-139, doi:10.1038/nature18010 (2016).
790 42 Hsia, Y. *et al.* Corrigendum: Design of a hyperstable 60-subunit protein icosahedron.
791 *Nature* **540**, 150, doi:10.1038/nature20108 (2016).
792 43 Zakeri, B. *et al.* Peptide tag forming a rapid covalent bond to a protein, through
793 engineering a bacterial adhesin. *Proc Natl Acad Sci U S A* **109**, E690-697,
794 doi:10.1073/pnas.1115485109 (2012).
795 44 Punjani, A., Rubinstein, J. L., Fleet, D. J. & Brubaker, M. A. cryoSPARC: algorithms for
796 rapid unsupervised cryo-EM structure determination. *Nat Methods* **14**, 290-296,
797 doi:10.1038/nmeth.4169 (2017).
798 45 Bepler, T. *et al.* Positive-unlabeled convolutional neural networks for particle picking in
799 cryo-electron micrographs. *Nat Methods* **16**, 1153-1160, doi:10.1038/s41592-019-0575-
800 8 (2019).
801 46 Rubinstein, J. L. & Brubaker, M. A. Alignment of cryo-EM movies of individual particles
802 by optimization of image translations. *J Struct Biol* **192**, 188-195,
803 doi:10.1016/j.jsb.2015.08.007 (2015).
804 47 Pettersen, E. F. *et al.* UCSF ChimeraX: Structure visualization for researchers,
805 educators, and developers. *Protein Sci* **30**, 70-82, doi:10.1002/pro.3943 (2021).

806 48 Liebschner, D. *et al.* Macromolecular structure determination using X-rays, neutrons and
807 electrons: recent developments in Phenix. *Acta Crystallogr D Struct Biol* **75**, 861-877,
808 doi:10.1107/S2059798319011471 (2019).
809 49 Emsley, P., Lohkamp, B., Scott, W. G. & Cowtan, K. Features and development of Coot.
810 *Acta Crystallogr D Biol Crystallogr* **66**, 486-501, doi:10.1107/S0907444910007493
811 (2010).
812 50 Williams, C. J. *et al.* MolProbity: More and better reference data for improved all-atom
813 structure validation. *Protein Sci* **27**, 293-315, doi:10.1002/pro.3330 (2018).
814 51 Reed, L. J. & Muench, H. A SIMPLE METHOD OF ESTIMATING FIFTY PER CENT
815 ENDPOINTS12. *American Journal of Epidemiology* **27**, 493-497,
816 doi:10.1093/oxfordjournals.aje.a118408 (1938).
817 52 Patel, D. R. *et al.* Transmission and Protection against Reinfection in the Ferret Model
818 with the SARS-CoV-2 USA-WA1/2020 Reference Isolate. doi:10.1128/jvi.02232-20
819 (2021).
820 53 Dhakal, S. *et al.* Sex Differences in Lung Imaging and SARS-CoV-2 Antibody
821 Responses in a COVID-19 Golden Syrian Hamster Model. *mBio* **12**, e0097421,
822 doi:10.1128/mBio.00974-21 (2021).
823 54 Field, C. J. *et al.* Immune durability and protection against SARS-CoV-2 re-infection in
824 Syrian hamsters. *Emerg Microbes Infect* **11**, 1103-1114,
825 doi:10.1080/22221751.2022.2058419 (2022).
826 55 Gerhards, N. M. *et al.* Predictive Value of Precision-Cut Lung Slices for the Susceptibility
827 of Three Animal Species for SARS-CoV-2 and Validation in a Refined Hamster Model.
828 *Pathogens* **10**, doi:10.3390/pathogens10070824 (2021).
829 56 Rosenthal, P. B. & Henderson, R. Optimal determination of particle orientation, absolute
830 hand, and contrast loss in single-particle electron cryomicroscopy. *J Mol Biol* **333**, 721-
831 745, doi:10.1016/j.jmb.2003.07.013 (2003).

832 57 Prisant, M. G., Williams, C. J., Chen, V. B., Richardson, J. S. & Richardson, D. C. New
833 tools in MolProbity validation: CaBLAM for CryoEM backbone, UnDowser to rethink
834 "waters," and NGL Viewer to recapture online 3D graphics. *Protein Sci* **29**, 315-329,
835 doi:10.1002/pro.3786 (2020).
836 58 Cohen, A. A. *et al.* Mosaic RBD nanoparticles protect against challenge by diverse
837 sarbecoviruses in animal models. *Science* **377**, eabq0839, doi:10.1126/science.abq0839
838 (2022).
839 59 Karimzadeh, S., Bhopal, R. & Nguyen Tien, H. Review of infective dose, routes of
840 transmission and outcome of COVID-19 caused by the SARS-COV-2: comparison with
841 other respiratory viruses. *Epidemiol Infect* **149**, e96, doi:10.1017/S0950268821000790
842 (2021).
843 60 Prentiss, M., Chu, A. & Berggren, K. K. Finding the infectious dose for COVID-19 by
844 applying an airborne-transmission model to superspreader events. *PLoS One* **17**,
845 e0265816, doi:10.1371/journal.pone.0265816 (2022).
846 61 Rosenke, K. *et al.* Defining the Syrian hamster as a highly susceptible preclinical model
847 for SARS-CoV-2 infection. *https://doi.org/10.1080/22221751.2020.1858177*, doi:Temi-
848 2020-1569.R1 (2020).
849 62 Focosi, D., Maggi, F. & Casadevall, A. Mucosal Vaccines, Sterilizing Immunity, and the
850 Future of SARS-CoV-2 Virulence. *Viruses* **14**, 187, doi:10.3390/v14020187 (2022).
851 63 Chavda, V. P., Vora, L. K., Pandya, A. K. & Patravale, V. B. Intranasal vaccines for
852 SARS-CoV-2: From challenges to potential in COVID-19 management. *Drug Discov*
853 *Today* **26**, 2619-2636, doi:10.1016/j.drudis.2021.07.021 (2021).
854 64 Bachmann, M. F. & Jennings, G. T. Vaccine delivery: a matter of size, geometry, kinetics
855 and molecular patterns. *Nature Reviews Immunology* **10**, 787-796,
856 doi:doi:10.1038/nri2868 (2010).

857 65 Ueda, G. *et al.* Tailored design of protein nanoparticle scaffolds for multivalent
858 presentation of viral glycoprotein antigens. *Elife* **9**, doi:10.7554/eLife.57659 (2020).
859 66 He, L. *et al.* Single-component, self-assembling, protein nanoparticles presenting the
860 receptor binding domain and stabilized spike as SARS-CoV-2 vaccine candidates. *Sci*
861 *Adv* **7**, doi:10.1126/sciadv.abf1591 (2021).
862 67 Kang, Y. F. *et al.* Rapid Development of SARS-CoV-2 Spike Protein Receptor-Binding
863 Domain Self-Assembled Nanoparticle Vaccine Candidates. *ACS Nano* **15**, 2738-2752,
864 doi:10.1021/acsnano.0c08379 (2021).
865 68 Tan, T. K. *et al.* A COVID-19 vaccine candidate using SpyCatcher multimerization of the
866 SARS-CoV-2 spike protein receptor-binding domain induces potent neutralising antibody
867 responses. *Nature Communications* **12**, doi:10.1038/s41467-020-20654-7 (2021).
868 69 Cohen, A. A. *et al.* Construction, characterization, and immunization of nanoparticles
869 that display a diverse array of influenza HA trimers. *PLoS One* **16**, e0247963,
870 doi:10.1371/journal.pone.0247963 (2021).
871 70 Walls, A. C. *et al.* Elicitation of Potent Neutralizing Antibody Responses by Designed
872 Protein Nanoparticle Vaccines for SARS-CoV-2. *Cell* **183**, 1367-1382 e1317,
873 doi:10.1016/j.cell.2020.10.043 (2020).
874 71 Mao, T. *et al.* Unadjuvanted intranasal spike vaccine elicits protective mucosal immunity
875 against sarbecoviruses. *Science* **378**, eabo2523, doi:10.1126/science.abo2523 (2022).

876

877 **FIGURE LEGENDS**

878 **Figure 1. Single-particle analysis and Cryo-EM reconstruction of the apo cage used for**
879 **immunizations.** (A) A representative cryo-EM micrograph of apo cage particles (scale bar, 25
880 nm) is provided. (B) Examples of representative class averages from a 2D classification of the
881 particles extracted from cryo-EM micrographs are provided. (C) A reconstructed icosahedral
882 map of the apo cage structure is colored according to the estimated local resolution; color key is
883 shown to the left of the map. Red numbers in gray boxes on the structural model indicate the
884 two-, three- and five-fold symmetry axes of the dodecahedron. Apo cage particles have an
885 approximate diameter of 25 nm. (D) A fourier shell correlation (FSC) curve of the reconstructed
886 map using gold-standard refinement in cryoSPARC is presented. An approximate map
887 resolution of 3.4 Å based on 0.143 FSC cutoff is indicated. (E) An atomic model of the apo cage
888 was built by applying icosahedral symmetry in ChimeraX to an asymmetric unit fitted to the
889 density of the map shown in (C). (F) Left: A portion of the map covering a single I3-01 monomer
890 is rendered as a transparent surface, with the fitted model (aa 22-222) shown as a light blue
891 cartoon with side chains represented as sticks. Right: A close-up view of residues Val183,
892 Cys184 and the C-terminal helix (aa 205-222) showing clear density of the assigned sidechains
893 is shown with the map contoured at level 0.9 in ChimeraX. The quality of density is sufficient to
894 observe the disulfide bond between Cys184 and the C-terminal Cys222.

895

896 **Figure 2. Display of RBD via the SpyCage scaffold.** (A) A schematic of the SpyCage scaffold
897 illustrates 6xHis purification tags, the SpyCatcher capture domain, a flexible linker, and a C-
898 terminal I3-01 variant used to create the self-assembling protein wireframe platform. A
899 schematic of RBD with a C-terminal 6xHis tag and with/without a C-terminal SpyTag is shown.
900 (B) SDS-PAGE of SpyCage, RBD, SpyCage+RBD, and SpyCage|RBD preparations. The
901 covalent bonding ("grafting") of RBD to SpyCage is evident when RBD bears a SpyTag, but not
902 in its absence as per a mobility shift. SpyCage approaches saturation with RBD at a 1-to-1.2

903 molar ratio of SpyCage-to-RBD, as has been seen with other antigens of comparable shape and
904 mass.
905
906 **Figure 3. Binding and neutralizing antibody responses to intranasal vaccination with**
907 **RBD+SpyCage.** Antibody titers were measured in serum samples on days 0, 28, and 55, prior
908 to primary vaccination, boost vaccination, and viral challenge, respectively. Plotted are (A) anti-
909 RBD IgG, (B) IgA titers, (C) neutralizing antibody titers against SARS-CoV-2, and (D) IgG
910 antibody titers against the SpyCage scaffold. * significantly different from all other groups by
911 Kruskal-Wallis with Dunn's multiple comparison. † significantly different from mock and RBD
912 groups.
913
914 **Figure 4. Weight loss and viral titers in the nasal turbinates and lungs after SARS-CoV-2**
915 **challenge of vaccinated hamsters.** After viral challenge, hamsters were monitored for (A)
916 weight loss, and viral titers were evaluated in (B) nasal turbinates and (C) lung tissues on days
917 3, 5 and 7 post-infection. *significantly different from RBD and RBD|Spycage. **significantly
918 different from RBD|SpyCage. Non-parametric Kruskal-Wallis test with Dunn's multiple
919 comparisons were used to determine significant differences.
920
921 **Figure 5. SARS-CoV-2 induced lung pathology in vaccinated hamsters.** On days 3, 5, and
922 7, post-infection, lung tissues were processed for H&E staining and scored by a veterinary
923 pathologist. Panel (A) displays representative images from each group of hamsters on days 5
924 and 7 post-infection. This panel also includes images of uninfected hamster lung tissues (far
925 right panels). Panels (B) and (C) display total pathology scores and the extent of lesions
926 scoring, respectively.

Patel *et al*. Figure 1

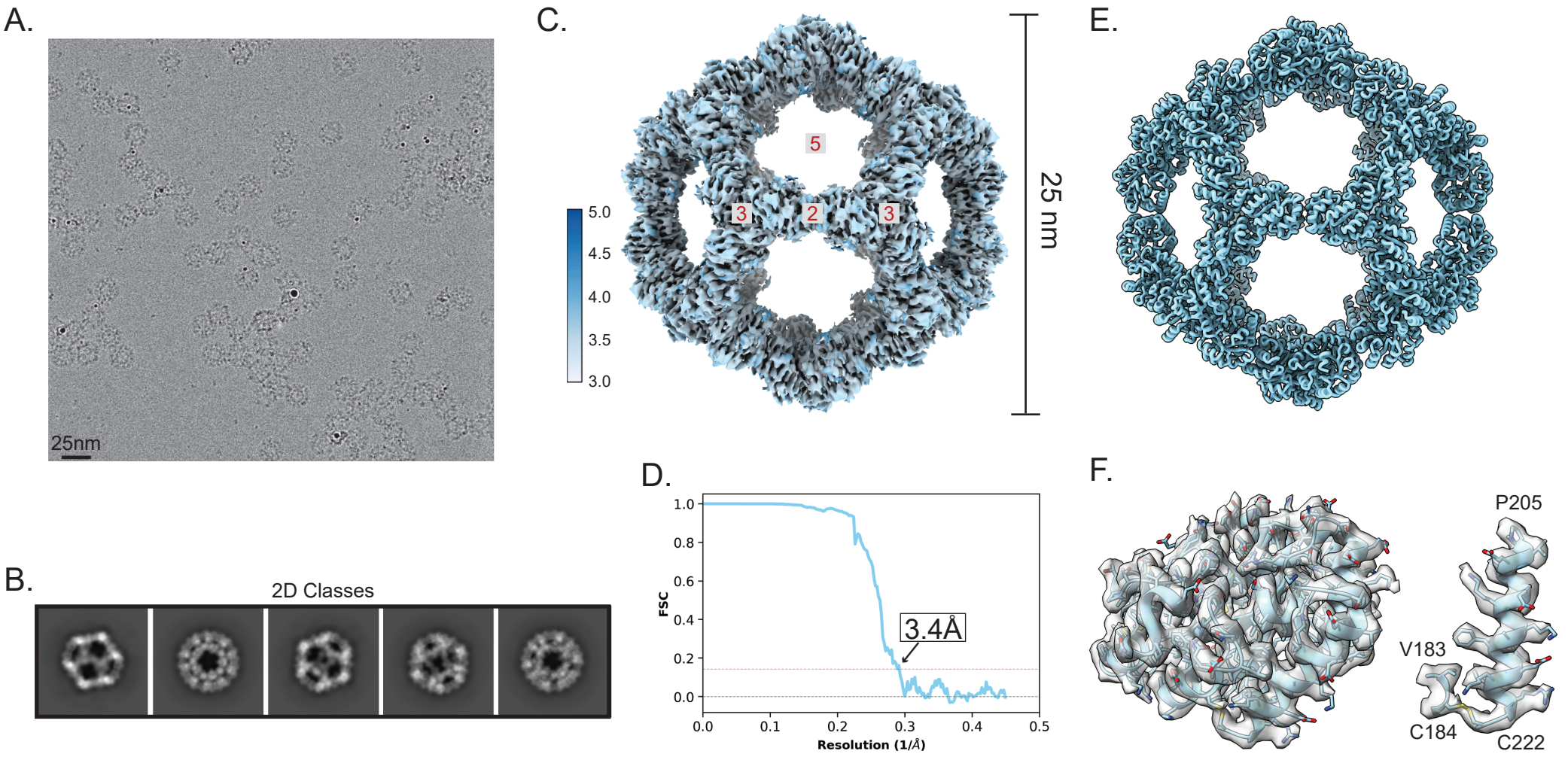

Patel *et al*. Figure 2

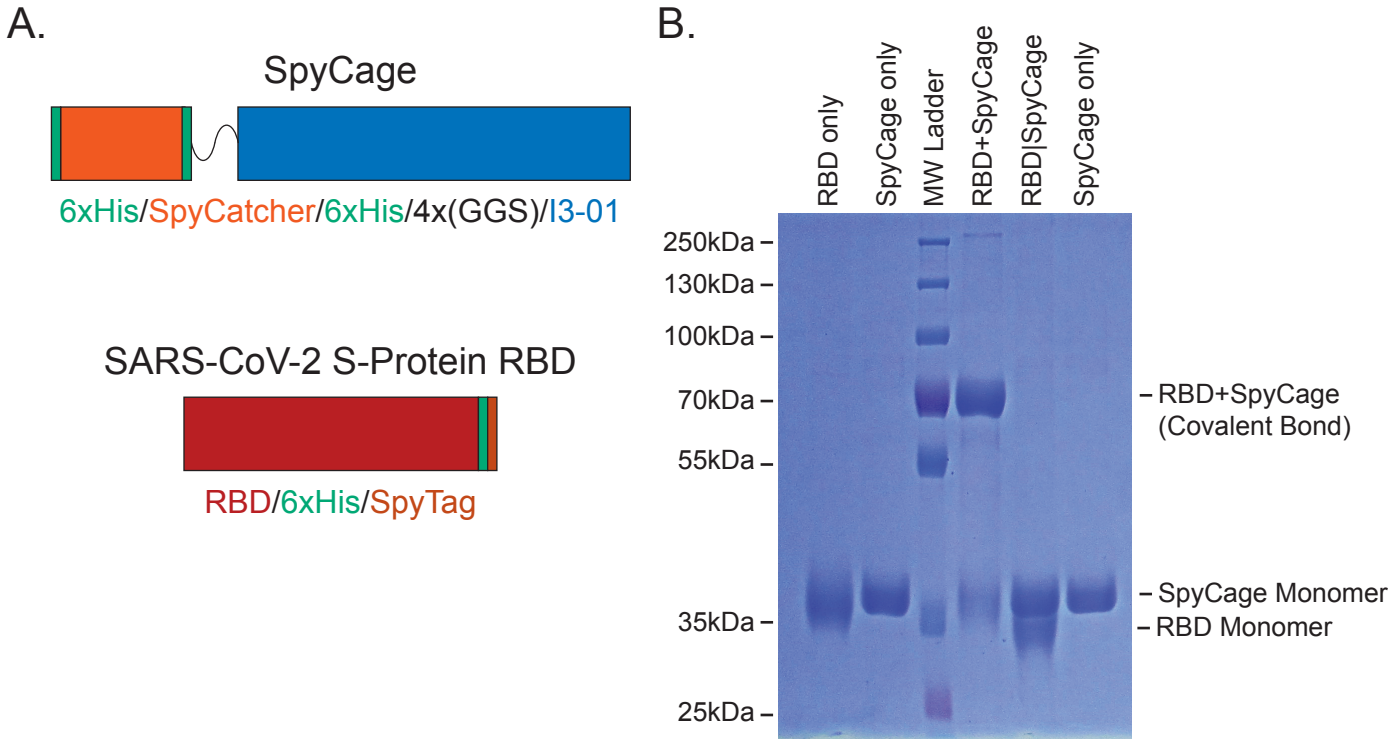

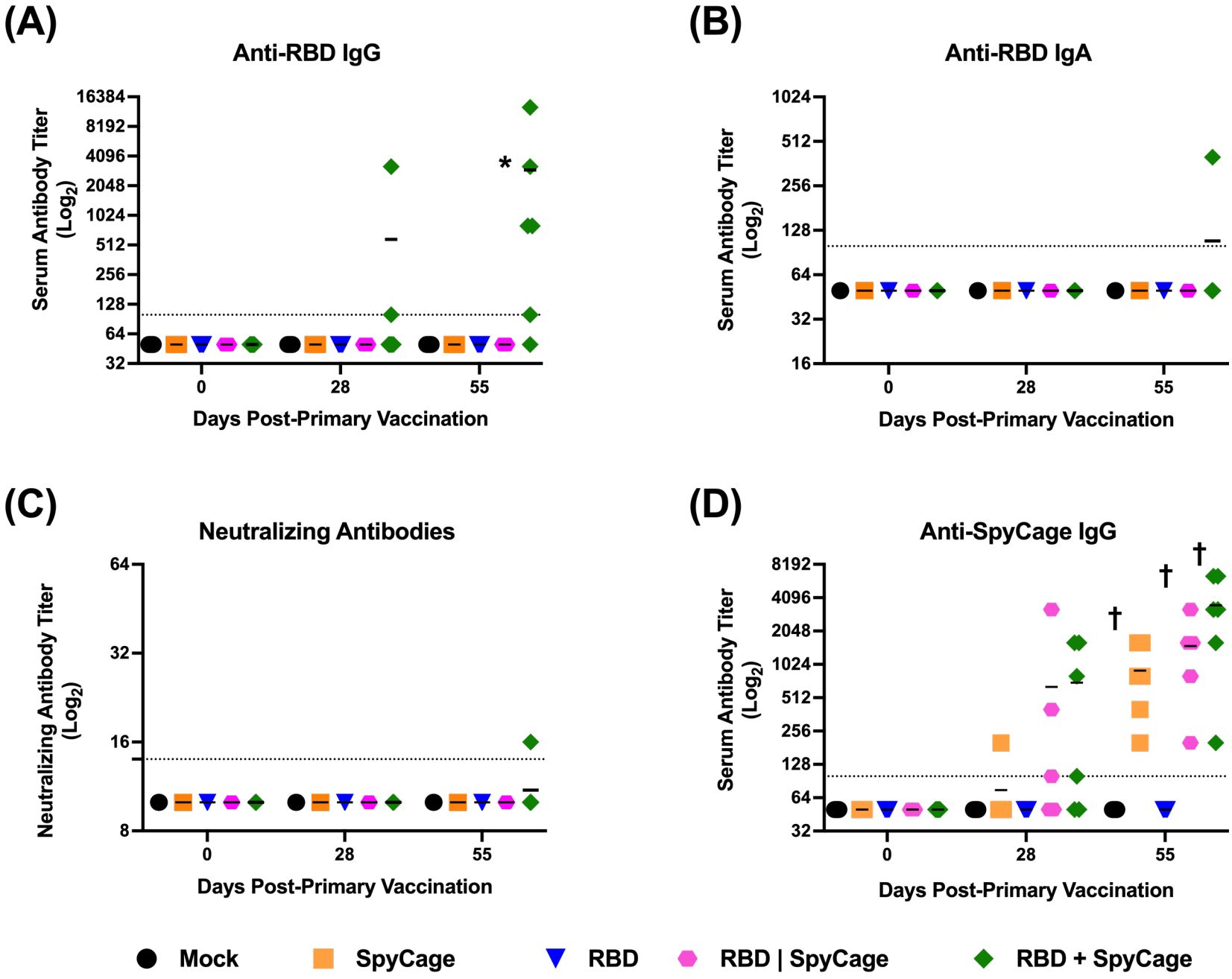
(A)
Anti-RBD IgG
Serum Antibody Titer (Log2)
16384
8192
4096
2048
1024
512
256
128
64
32
*
0
28
55
Days Post-Primary Vaccination
(B)
Anti-RBD IgA
Serum Antibody Titer (Log2)
1024
512
256
128
64
32
16
0
28
55
Days Post-Primary Vaccination
(C)
Neutralizing Antibodies
Neutralizing Antibody Titer (Log2)
64
32
16
8
0
28
55
Days Post-Primary Vaccination
(D)
Anti-SpyCage IgG
Serum Antibody Titer (Log2)
8192
4096
2048
1024
512
256
128
64
32
†
†
†
0
28
55
Days Post-Primary Vaccination
Mock
SpyCage
RBD
RBD | SpyCage
RBD + SpyCage

Figure 3

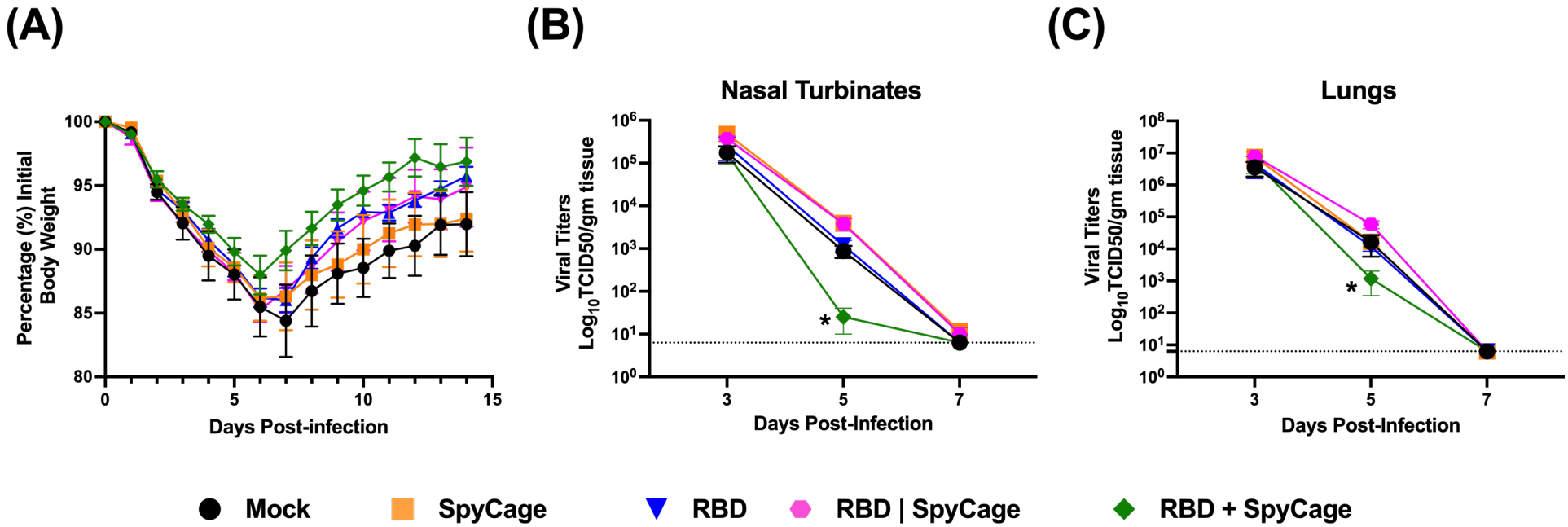
(A)
(B)
(C)
Nasal Turbinates
Lungs
Percentage (%) Initial Body Weight
Viral Titers Log10TCID50/gm tissue
Days Post-infection
Days Post-Infection
Mock
SpyCage
RBD
RBD | SpyCage
RBD + SpyCage

Figure 4

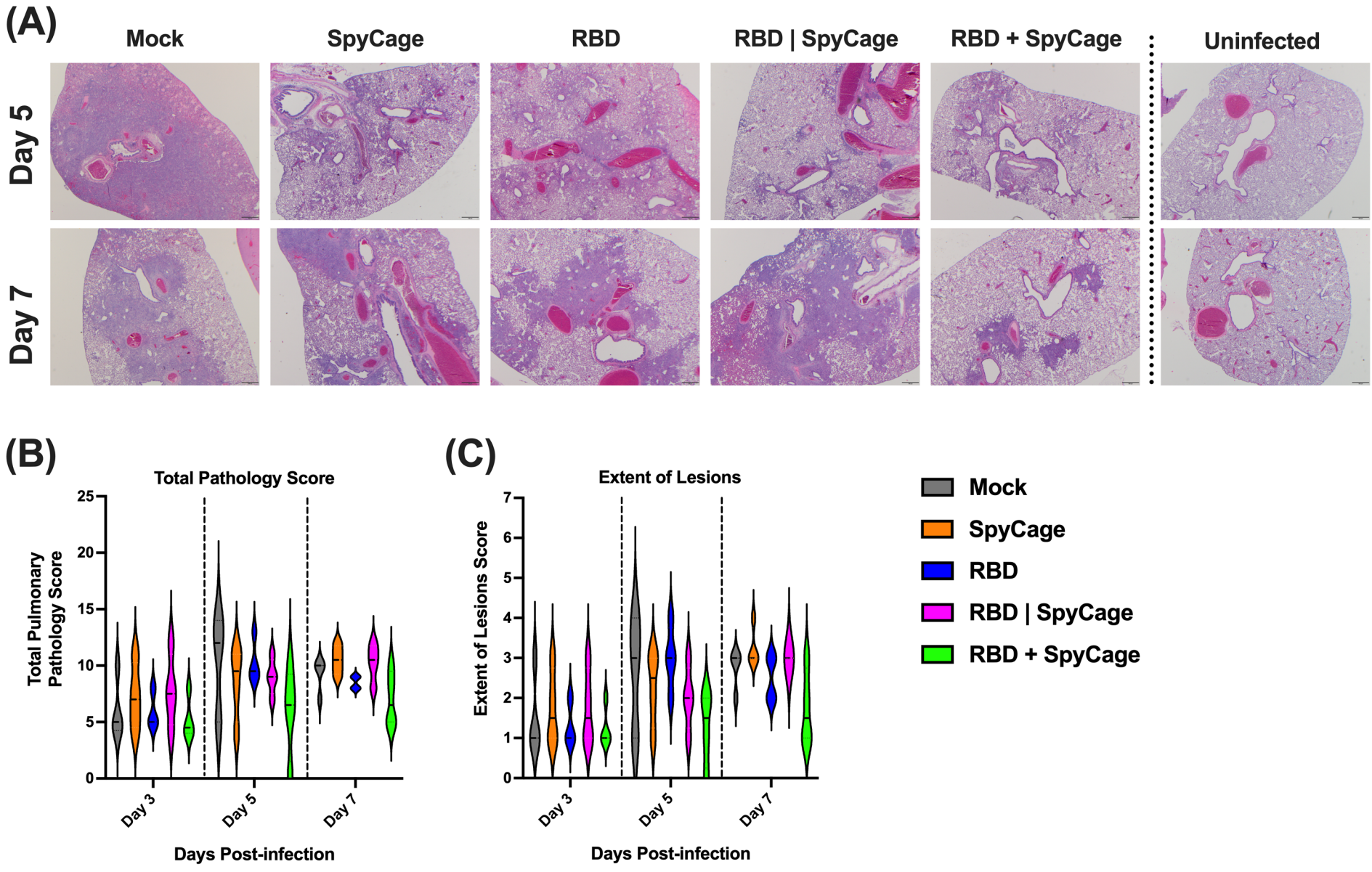
(A)
Mock
SpyCage
RBD
RBD | SpyCage
RBD + SpyCage
Uninfected
Day 5
Day 7
(B)
Total Pathology Score
Total Pulmonary Pathology Score
25
20
15
10
5
0
Day 3
Day 5
Day 7
Days Post-infection
(C)
Extent of Lesions
Extent of Lesions Score
7
6
5
4
3
2
1
0
Day 3
Day 5
Day 7
Days Post-infection
Mock
SpyCage
RBD
RBD | SpyCage
RBD + SpyCage

Figure 5